Higher Hydroclimatic Intensity with Global Warming

F. GIORGI, E.-S. IM, AND E. COPPOLA

Earth System Physics Section, International Centre for Theoretical Physics, Trieste, Italy

N. S. DIFFENBAUGH

Department of Environmental Earth System Science, and Woods Institute for the Environment, Stanford University, Stanford, California

X. J. GAO

National Climate Center, Chinese Meteorological Administration, Beijing, China

L. MARIOTTI

Earth System Physics Section, International Centre for Theoretical Physics, Trieste, Italy

Y. SHI

National Climate Center, Chinese Meteorological Administration, Beijing, China

(Manuscript received 5 August 2010, in final form 13 March 2011)

ABSTRACT

Because of their dependence on water, natural and human systems are highly sensitive to changes in the hydrologic cycle. The authors introduce a new measure of hydroclimatic intensity (HY-INT), which integrates metrics of precipitation intensity and dry spell length, viewing the response of these two metrics to global warming as deeply interconnected. Using a suite of global and regional climate model experiments, it is found that increasing HY-INT is a consistent and ubiquitous signature of twenty-first-century, greenhouse gas–induced global warming. Depending on the region, the increase in HY-INT is due to an increase in precipitation intensity, dry spell length, or both. Late twentieth-century observations also exhibit dominant positive HY-INT trends, providing a hydroclimatic signature of late twentieth-century warming. The authors find that increasing HY-INT is physically consistent with the response of both precipitation intensity and dry spell length to global warming. Precipitation intensity increases because of increased atmospheric water holding capacity. However, increases in mean precipitation are tied to increases in surface evaporation rates, which are lower than for atmospheric moisture. This leads to a reduction in the number of wet days and an increase in dry spell length. This analysis identifies increasing hydroclimatic intensity as a robust integrated response to global warming, implying increasing risks for systems that are sensitive to wet and dry extremes and providing a potential target for detection and attribution of hydroclimatic changes.

1. Introduction

Global warming has been scientifically established as unequivocal and almost certainly caused by human activities (Solomon et al. 2007). Water is critical for most aspects of the earth's biosphere and human societies, and thus the most acute impacts of global warming are likely to be felt through changes in the hydrologic cycle (Bates et al. 2008). Of particular concern is the possibility that global warming causes the hydrologic cycle to accelerate, thereby increasing the intensity of both wet and dry extremes (Hennessy et al. 1997; Dai et al. 1998; Trenberth 1999; Allen and Ingram 2002; Trenberth et al. 2003; Christensen and Christensen 2003; Held and Soden 2006; Allan and Soden 2008). If true, this acceleration

Corresponding author address: Filippo Giorgi, Earth System Physics Section, International Centre for Theoretical Physics, Strada Costiera 11, 34100 Trieste, Italy.
E-mail: giorgi@ictp.it

DOI: 10.1175/2011JCLI3979.1

© 2011 American Meteorological Society

TABLE 1. Description of models used for the analysis of Figs. 2 and 3. Note that for each regional model run the corresponding driving global model is indicated.

	Institute	Model	Resolution	Period	Reference period	Reference
Global projection	Max Planck Institute (MPI)	ECHAM5	1.9°	1961–2100	1961–2000	World Climate Research Programme (WCRP),
	National Center for Atmospheric Research (NCAR)	CCSM	1.4°	1950–2099	1950–2000	Climate Model Intercomparison Project 3 (CMIP3)
	MRI	Coupled General Circulation Model (CGCM)	2.8°	1961–2000 2046–65 2081–2100	1961–2000	multimodel data (https://esg.llnl.gov:8443/)
Regional projection (Europe)	ICTP	ECHAM5-RegCM3	25 km	1951–2100	1951–2000	Ensemble-Based Predictions of Climate Changes and their Impacts (ENSEMBLES) (http://ensemblesrt3.dmi.dk/)
	Hadley Centre (HC)	Third climate configuration of the Met Office Unified Model (HadCM3Q)-HadRM3P	25 km	1951–2099	1951–2000	
	Centre National de Recherches Météorologiqu es (CNRM)	Action de Recherche Petite Echelle Grande Echelle (ARPEGE)-ALADIN	25 km	1951–2100	1951–2000	
Regional projection (Africa)	ICTP	ECHAM5-RegCM3	50 km	1980–2100	1980–2000	ENSEMBLES (http://ensemblesrt3.dmi.dk/)
	HC	HadCM3Q-HadRM3P	50 km	1951–2099	1951–2000	
Regional projection (East Asia)	ICTP	ECHAM5-RegCM3	60 km	1971–2100	1971–2000	Im et al. 2011
	China Meteorological Administration (CMA)	Model for Interdisciplinary Research on Climate 3.2, high-resolution version (MIROC_hires)-RegCM3	25 km	1951–2100	1951–2000	X. Gao 2009, personal communication
Regional projection (North America)	Purdue/Stanford	CCSM3-RegCM3	25 km	1951–2099	1951–2000	Diffenbaugh and Ashfaq 2010

should be seen in climate model experiments that test the response of the climate system to elevated greenhouse gas (GHG) forcing, and in observations that record the climate system response to recent changes in global mean temperature (TMP). If this hydroclimatic signature is found in model experiments and instrumental observations, then the imprint of global warming on the earth's hydroclimate can provide a powerful tool to detect and assess the climatic effects of anthropogenic GHG emissions.

Climate projections for the twenty-first century indicate a global-scale increase in precipitation intensity (INT) and number of dry days in response to increased GHG concentrations, although with pronounced regional variability (Solomon et al. 2007). To date, these wet and dry features have mostly been approached separately, with particular emphasis on the response of dry and wet extremes to warming (Trenberth 1999; Allen and Ingram 2002; Meehl et al. 2005; Tebaldi et al. 2006; Dai et al. 2004; O'Gorman and Schneider 2009; Sugiyama et al. 2010). However, it is likely that the processes governing the increase in wet and dry events are deeply interconnected, and manifestations of the same underlying hydroclimatic response (Trenberth 1999; Trenberth et al. 2003).

Within this integrated view, we introduce a single index that quantitatively combines measures of precipitation intensity and dry spell length, thereby providing an overall metric of hydroclimatic intensity. An increase of this index, which we name the hydroclimatic intensity (or HY-INT; see section 2) index, would indicate an increase in the occurrence of heavy precipitation events or dry spell length, or a combined increase in both. GHG-induced changes in HY-INT that are found to be robust can thus be considered as specific integrated hydroclimatic signatures of global warming, and can provide valuable information in detecting, understanding, and

TABLE 2. Regional observation and global reanalysis datasets used for analysis of Figs. 1, 4, and 5.

		Data type	Resolution	Period	Reference
Global reanalysis	NCEP	Grid	1.875°	1950–2000	Kalnay et al. 1996
	ERA-40	Grid	2.5°	1958–2000	Uppala et al. 2005
Europe		Grid	25 km	1950–2000	Haylock et al. 2008
Africa		Station	460 stations	1961–96	GCOS (http://www.ncdc.noaa.gov/oa/climate/ghcn-daily/)
India and East Asia		Grid	0.25°	1961–2000	Yatagai et al. 2009
Australia		Station	59 stations	1961–2000	GCOS (http://www.ncdc.noaa.gov/oa/climate/ghcn-daily/)
North America		Station	2551 stations	1961–2000	GCOS (http://www.ncdc.noaa.gov/oa/climate/ghcn-daily/)
South America		Grid	1°	1978–2000	Silva et al. 2007

attributing changes in the earth's hydrologic cycle. Toward this goal, in this paper we present an analysis of HY-INT trends in a suite of global and regional climate model experiments of GHG-induced global warming and in a set of precipitation observation datasets for the late decades of the twentieth century.

In section 2 we first describe the HY-INT index and discuss the rationale for its choice. In section 3 we analyze the global and regional model projections of climate change for the twenty-first century to identify a robust response of HY-INT to GHG-induced global warming conditions. We also place this response within the context of the changes induced by global warming on the earth's hydrologic cycle. In section 4 we search for a HY-INT signature in hydroclimatic observations of the latest decades of the twentieth century. Finally, in section 5 we present a discussion of the implications of our findings for the assessment of the effects of global warming on the earth's hydrologic cycle.

2. The HY-INT index, data, and methods

To calculate HY-INT, we first compute the mean annual precipitation intensity (intensity during wet days) and the mean annual dry spell length (DSL; number of consecutive dry days during each dry spell). A day is defined as ''dry'' (''wet'') if the daily precipitation amount is below (above) 1 mm (Salinger and Griffiths 2001). We then normalize both INT and DSL by their mean value for the twentieth-century period of available data (see Tables 1 and 2a). (We note that although the reference period varies based on data availability, the exact reference period is not essential as it only serves to normalize the values of INT and DSL.) The value of HY-INT for a given year and location is then simply given by

$$\text{HY-INT} = \text{INT} \times \text{DSL}. \tag{1}$$

From Eq. (1) it is evident that HY-INT increases if INT and DSL increase or if the increase in one of them overwhelms the decrease in the other. Therefore, an increase of HY-INT measures a dominant increase of INT, DSL, or both. In fact, larger increases of HY-INT would occur when both INT and DSL increase and this would register a change in the characteristics of the hydrologic cycle. For example, if the mean precipitation (PRE) remained constant, but the mode of precipitation changed with less frequent but more intense events, this would be reflected in a strong response of HY-INT (with contributions from both INT and DSL). Hence, the rationale for the choice of Eq. (1) is that it measures combined changes in the properties of the hydrologic cycle related to the intensity and frequency of events, treating the response of these properties to global warming as inherently interconnected and thus amplifying signals associated with INT and DSL individually. Obviously, different functions could be used in place of Eq. (1) to measure this response, but Eq. (1) offers the advantage of being simple and readily computed from daily data.

One of the reviewers suggested the following physical interpretation of the HY-INT index: if one defines f_d (f_w), l_d (l_w), and n_d (n_w), the average frequency of dry (wet) days, average length of dry (wet) spells, and average number of dry (wet) spells, respectively, simple algebra yields the following dimensional definition of HY-INT:

$$\text{HY-INT} = (1/n_d)(P/f_w - P), \tag{2}$$

where P is mean precipitation. In turn, if $f_w = n_w l_w$ and $f_d = n_d l_d$, Eq. (2) can be written as

$$\text{HY-INT} = (P/n_w)(l_d/l_w). \tag{3}$$

By this interpretation, HY-INT is the average accumulated wet spell precipitation amount multiplied by the ratio between dry and wet spell mean duration. An increase in HY-INT would thus denote an increase in either or both of these quantities.

We also stress that HY-INT is not intended to be an index of precipitation or drought extremes (as it could increase also if the mean intensity of light events increases), but rather an index of overall hydroclimatic

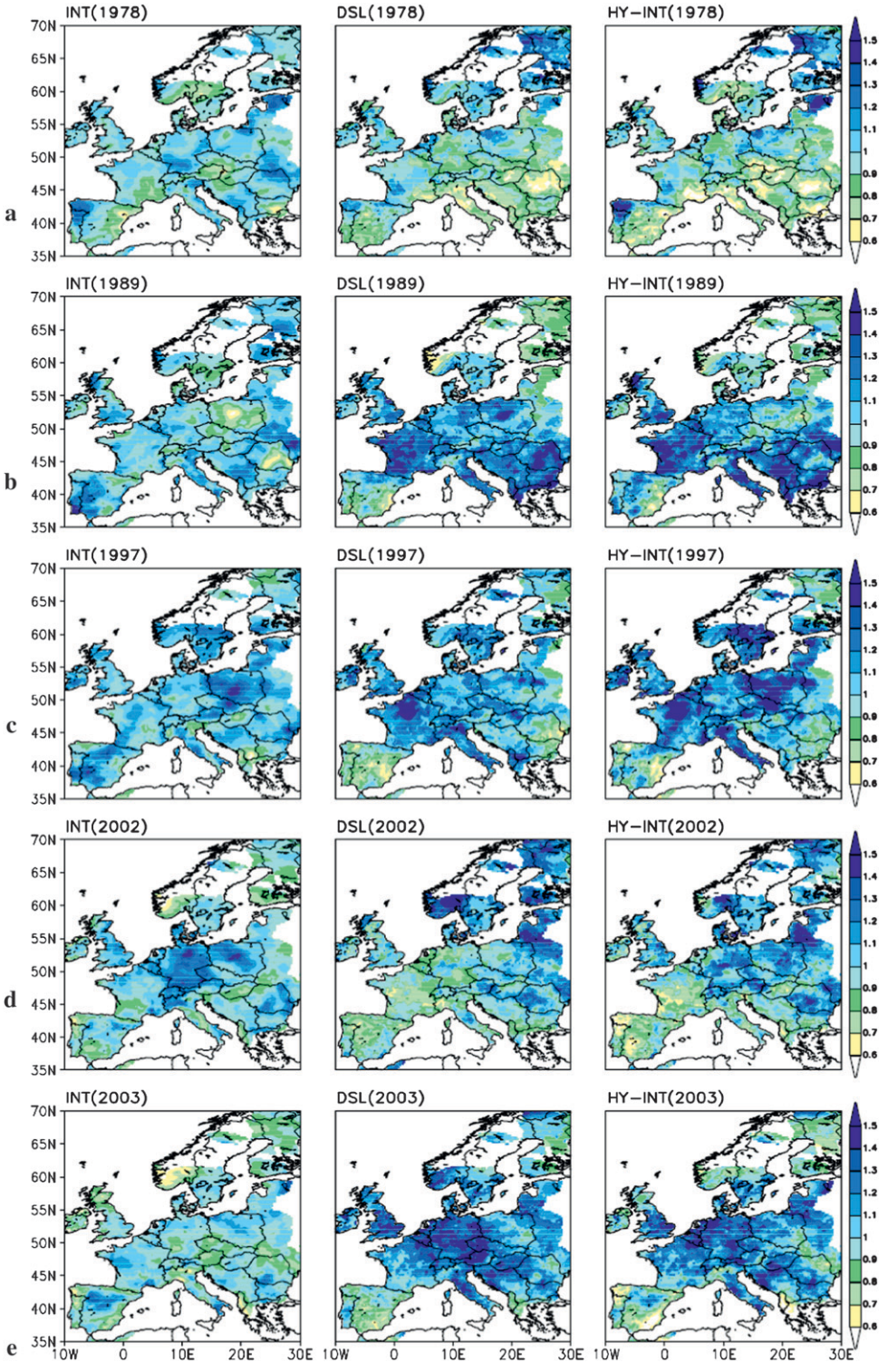

FIG. 1. Maps of observed (left to right) INT, DSL, and HY-INT over Europe for five illustrative years. (a) 1978: example of a year with relatively normal conditions; (b) 1989: example of a year with high HY-INT values over central and eastern Europe mostly due to relatively dry conditions (high DSL; Luterbacher et al. 2004); (c) 1997: example of a year with high HY-INT due to relatively dry conditions over France and Italy and wet conditions (high INT) over northeastern Europe (Barredo 2007); (d) 2002: example of a year with high HY-INT due to relatively wet conditions over central Europe (Barredo 2007); and (e) 2003: example of a year with high HY-INT due to relatively dry conditions over central Europe (Beniston 2004; Schär et al. 2004).

TABLE 3. Temperature (°C) and precipitation (%) changes (2071–2100 minus 1971–2000) averaged globally and over the continental regions (land only) of Fig. 2.

	Temperature change (°C)			Precipitation change (%)		
	ECHAM5	CCSM	MRI	ECHAM5	CCSM	MRI
Global	2.91	2.44	2.06	5.41	5.66	4.71
Europe	3.32	3.23	2.44	−0.78	2.92	4.38
Africa	4.14	2.91	2.68	5.53	11.83	1.55
India	4.20	3.00	2.62	5.44	10.84	17.19
East Asia	4.11	3.28	2.70	3.07	13.83	6.59
Australia	3.71	2.96	2.50	−8.48	4.49	0.94
North America	4.13	3.45	2.78	6.15	7.39	4.98
South America	3.72	2.64	2.11	3.44	6.99	1.33

intensity. On the other hand, an increase of HY-INT would generally indicate a higher risk of long drought spells and/or heavy precipitation events (see below).

We calculate HY-INT at individual points, either station observations or grid points, and then spatially average over individual points to obtain regional and global values. Illustrative maps of INT, DSL, and HY-INT for different years based on observed gridded precipitation over Europe (see below) are given in Fig. 1. The figure includes different illustrative cases: 1978 (Fig. 1a) is an example of a year with relatively normal conditions and low values of HY-INT; 1989 (Fig. 1b) is an example of a year with high HY-INT values over central and eastern Europe mostly due to relatively dry conditions (high DSL; Luterbacher et al. 2004); 1997 (Fig. 1c) is an example of a year with high HY-INT due to relatively dry conditions over France and Italy and wet conditions (high INT) over northeastern Europe (Barredo 2007); 2002 (Fig. 1d) is an example of a year with high HY-INT due to relatively wet conditions over central Europe (Barredo 2007); 2003 (Fig. 1e) is an example of a year with high HY-INT due to relatively dry conditions over central Europe (Beniston 2004; Schär et al. 2004). These examples show that, although HY-INT is calculated from annual statistics and is not a specific index of drought or flood, a high HY-INT value is a measure of a more intense hydrologic cycle due to the occurrence of more severe dry and/or wet events. They also show the utility of HY-INT as an integrator of dry and wet events.

In the next sections, we calculate HY-INT trends from three global model simulations for the twentieth and twenty-first centuries (Meehl et al. 2007b), a suite of regional climate model projections, and various station observation datasets. Tables 1 and 2 provide details of these various datasets. Trends in HY-INT are computed for two periods. For the twenty-first-century projections, we calculate a linear trend over the full 2001–2100 period. Here we consider projections for the A1B emission scenario, which lies near the middle of the Intergovernmental Panel on Climate Change Fourth Assessment Report (IPCC AR4) illustrative suite (Nakicenovic and Swart 2000). Given the scalability of projections of precipitation change (Giorgi 2008), we expect that the same conclusions apply to other scenarios as well. (We have indeed verified this scaling for the A2 scenario.) For the twentieth century, we calculate linear trends over the base period of 1976–2000, which was chosen both because it is a period common to most of the observation-based datasets we examine and because it is the period of the most pronounced anthropogenic GHG-induced twentieth-century warming (approximately 0.5°C) after the so-called climate shift (Solomon et al. 2007). However, to test the sensitivity of HY-INT to the choice of base period, we also calculate trends over other periods of the twentieth century (see Tables 6 and 7). We calculate the statistical significance of the trends using an F test Also, we note that for some observation datasets [e.g., Global Climate Observing System (GCOS)], some missing data are found. In this case, we only include stations with at least 300 days of available data during the analysis period, and we do not include in the analysis the days with missing data (i.e., dry sequences including missing days are not considered).

3. Response of HY-INT in global and regional warming projections for the twenty-first century

We first analyze global and regional climate model projections for the twenty-first century under the A1B GHG emissions scenario (see Tables 1 and 2). Table 3 reports the mean temperature and precipitation change by the end of the twenty-first century globally and over different continents for the three global models that we analyzed, while Fig. 2 presents twenty-first-century trends in HY-INT both at the gridpoint level for the whole globe (ECHAM5 simulation) and averaged over different continents. Corresponding trends in INT and DSL are reported in Table 4.

All three global climate models simulate statistically significant positive global trends of HY-INT in the twenty-first century. ECHAM5, the model with the largest

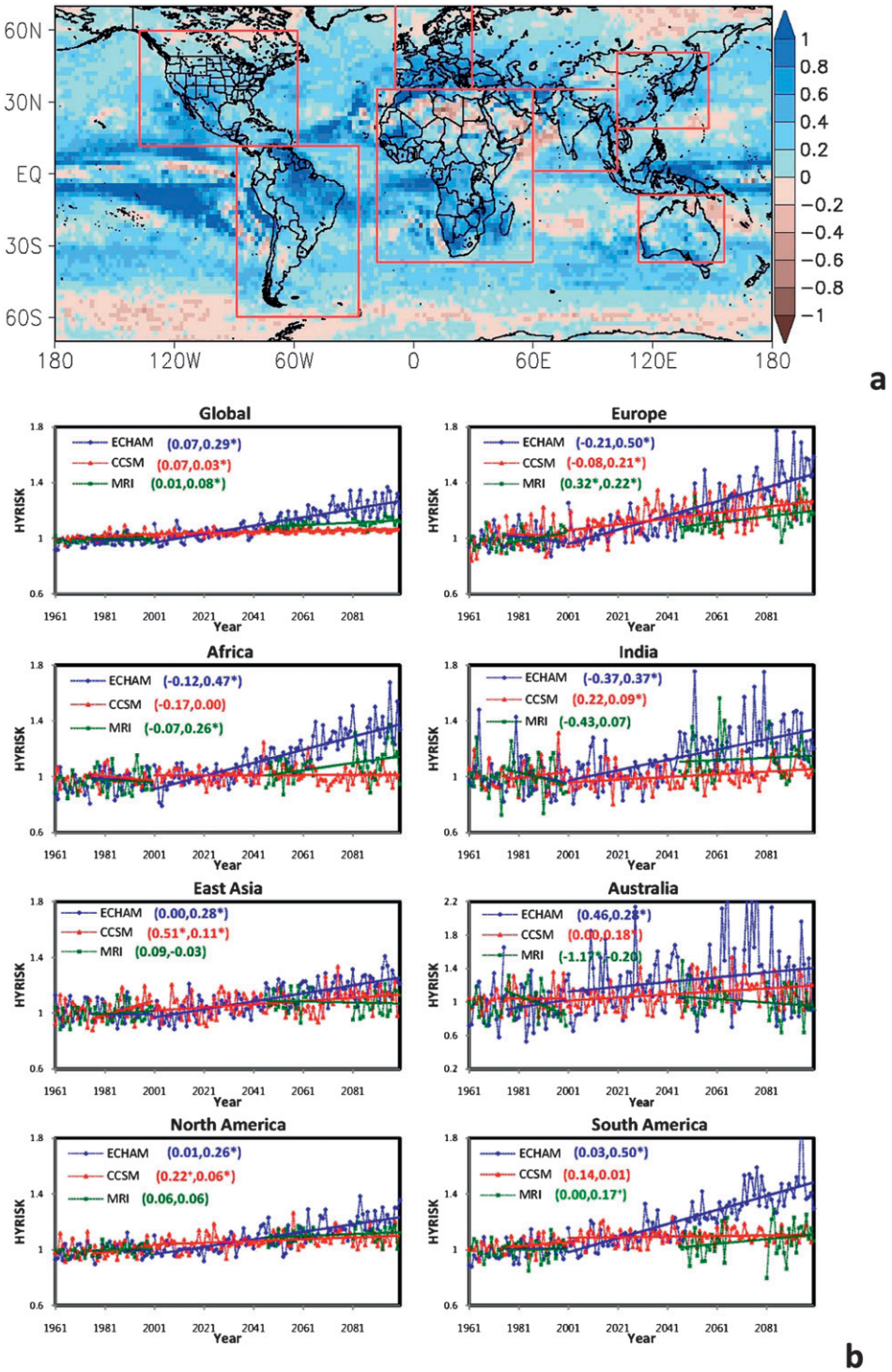

FIG. 2. HY-INT trends from global model projections: (a) spatial distribution of the twenty-first-century linear trend in HY-INT derived from the ECHAM5 A1B projection; (b) temporal evolution of the twenty-first-century HY-INT averaged globally and over the different continental regions depicted by the boxes in (a) (land only) derived from three coupled global models (Meehl et al. 2007b) [ECHAM5, CCSM, and the Meteorological Research Institute (MRI)] (see Table 1). Note that for MRI only two 20-yr time slices of daily data were available (2046–55 and 2081–2100) and are shown; and are used to estimate the twenty-first-century long linear trends by omitting missing years. The linear trend lines for the 1976–2000 and 2001–2100 periods are shown for each region. The legend indicates the linear trend value for 1976–2000 (first value) and 2001–2100 (second value) and the asterisk (cross) denotes statistical significance at the 95% (90%) confidence level.

TABLE 4. Linear trend coefficients of normalized INT and DSL in three global model projections (see Table 1) for the periods 1976–2000 and 2001–2100 (A1B scenario) averaged globally and over the continental regions of Fig. 2 (land only). Here, the asterisk and cross indicate that the trends are statistically significant at the 95% and 90% confidence levels, respectively.

		ECHAM5		CCSM		MRI	
		1976–2000	2001–2100	1976–2000	2001–2100	1976–2000	2001–2100
INT	Global	0.00	0.15*	0.02	0.04*	0.01	0.07*
	Europe	0.00	0.11*	0.17^{+}	0.07*	0.03	0.10*
	Africa	−0.09	0.16*	0.13^{+}	0.06*	0.09	0.15*
	India	−0.08	0.18*	0.07	0.06*	0.00	0.22*
	East Asia	0.01	0.18*	0.10	0.12*	0.10	0.06*
	Australia	−0.07	0.18*	0.12	0.03*	0.00	0.21^{+}
	North America	0.10^{+}	0.15*	−0.09^{+}	0.04*	0.02	0.07*
	South America	0.03	0.19*	0.05	0.05*	0.04	0.04*
DSL	Global	0.05	0.16*	0.05	0.00	−0.01	0.01
	Europe	−0.23	0.37*	−0.25	0.14*	0.28*	0.09
	Africa	−0.05	0.30*	−0.33*	−0.04^{+}	−0.28	0.08
	India	−0.30	0.19*	0.14	0.03	−0.40	−0.08
	East Asia	−0.03	0.08*	0.40*	0.00	0.00	−0.10
	Australia	0.62	0.04	−0.14	0.13*	−1.29^{+}	−0.49*
	North America	−0.08	0.09*	0.31*	0.01	0.02	0.00
	South America	0.00	0.25*	0.09	−0.04*	−0.07	0.11

temperature response (Table 3), shows the maximum trend [0.29 (100 yr)$^{-1}$], while the Community Climate System Model (CCSM) shows the minimum trend [0.03 (100 yr)$^{-1}$] (Fig. 2, Table 4). Note that the models with larger (smaller) trends also exhibit larger (smaller) interannual variability of HY-INT. Figure 2 shows that there is substantial regional variability in the twenty-first-century HY-INT trends, although positive values are found over most of the globe. In the ECHAM5 simulation, particularly high twenty-first-century HY-INT trends are found over Europe, the Amazon basin, the southwestern United States, southern and western Africa, Southeast Asia, and some equatorial oceanic regions. Figure 2 also shows that almost all continental-scale HY-INT trends are positive and statistically significant. We also note that all models show a twenty-first-century increase in global mean precipitation (Table 3) along with a global increase in both INT and DSL (except for the negligible trend in DSL for CCSM) (Table 4). At the continental scale, twenty-first-century trends in INT are all positive and statistically significant, while more mixed trend signals are found for DSL.

Our ensemble of high-resolution regional climate model projections shows a clear increasing trend in HY-INT for all regions and all models considered (Fig. 3). The magnitude of the trends is fairly consistent across models and regions [(0.15–0.32) (100 yr)$^{-1}$], and the majority of trends is statistically significant. Table 5 presents the corresponding regional trends in INT and DSL. For both variables, the majority of trends is positive and statistically significant, with only a few exceptions. The European region presents a particularly interesting case, where precipitation is projected to increase over central and northern Europe and decrease over the Mediterranean region (e.g., Giorgi and Coppola 2007). This dipolar response is also seen in the HY-INT metric, with increasing precipitation intensity mostly dominating over northern Europe, and increasing dry spell length dominating over southern Europe (Table 5). In both cases, the result is an increase in HY-INT of comparable magnitude.

Based on this suite of twenty-first-century climate model projections, we can conclude that an increase of HY-INT is a robust and ubiquitous hydroclimatic signature of GHG-induced global warming, both at the global and continental scales. This conclusion is supported by all global and regional climate model projections analyzed here. In the next subsection we place the HY-INT response identified here within the context of the response of the earth's hydrologic cycle to global warming.

HY-INT response within the context of the hydrologic cycle under global warming conditions

Starting from the consideration that the atmospheric moisture cycle is determined by an equilibrium between a slow and continuous evaporation (EVP) source and an intermittent removal by precipitation, it has been argued that precipitation events are mostly fed by atmospheric moisture transport in convergence areas surrounding synoptic and convective storm systems (Trenberth et al. 2003). As such, the intensity of precipitation is tied to the atmospheric moisture content, which is in turn regulated by the Clausius–Clapeyron (C–C) relationship, which implies an increase in atmospheric moisture holding capacity of approximately 7% (°C)$^{-1}$ of warming. The C–C

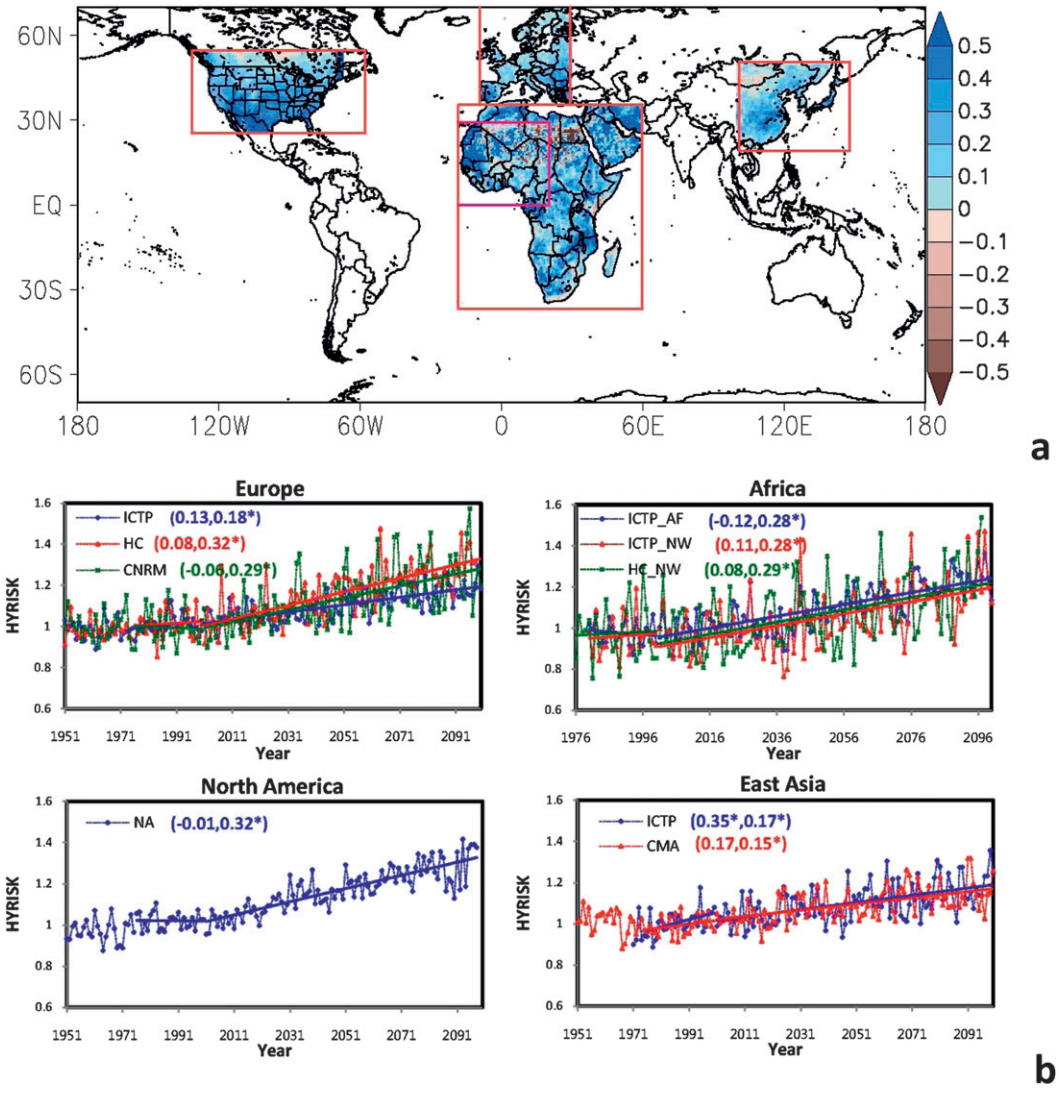

FIG. 3. HY-INT trends from regional model projections: (a) spatial distribution of the twenty-first-century linear trend in HY-INT derived from the Abdus Salam International Centre for Theoretical Physics (ICTP) regional climate model (RegCM; Pal et al. 2007) over different domains; (b) temporal evolution of HY-INT averaged over the different domains shown in (a) (land only) by three regional climate models [RegCM, Aire Limitée Adaptation Dynamique Développement International (ALADIN), and Hadley Centre Regional Model version 3P (HadRM3p) (see Table 1)]. The linear trend lines for the 1976–2000 and 2001–2100 periods are shown for each region. The legend indicates the linear trend coefficient for 1976–2000 (first value) and 2001–2100 (second value) and the asterisk (cross) denotes statistical significance at the 95% (90%) confidence level. In the top right panel of (b), AF denotes the all-Africa domain and NW the northwest Africa domain of (a).

dependence is especially strong for extreme precipitation events, which can substantially deplete the atmospheric moisture column (Allen and Ingram 2002; Trenberth et al. 2003; Allan and Soden 2008; Pall et al. 2007; Lenderink and Van Meijgaard 2008).

If mean precipitation increases less than precipitation intensity, the number of rainy days is reduced (Trenberth et al. 2003) and this leads to higher HY-INT. But what regulates the changes in mean precipitation? It has been suggested that a key factor is the ability of the troposphere to radiate away the energy released by condensed precipitation (Allen and Ingram 2002). On the other hand, if the relative humidity of the atmosphere remains relatively unchanged (Trenberth et al. 2003; Meehl et al. 2007a), the mean precipitation increase should be tied to the increase in evaporation from the warmer oceans and land. However, land areas do not evaporate at their potential rate, and in fact continental drying is found in most

TABLE 5. Linear trend coefficients of normalized INT and DSL in the regional model projections analyzed here (see Table 1) for the periods 1976–2000 and 2001–2100 (A1B scenario) averaged over the domains of Fig. 3 (land only). Here, asterisk and cross indicate that the trends are statistically significant at the 95% and 90% confidence levels, respectively.

			INT		DSL	
			1976–2000	2001–2100	1976–2000	2001–2100
Europe	ICTP	Whole	0.09^{+}	0.07*	0.04	0.11*
		South	0.17	0.02	0.23	0.24*
		North	0.04	0.11*	−0.11	0.00
	HC	Whole	−0.03	0.11*	0.11	0.20*
		South	−0.08	0.09*	0.34	0.33*
		North	0.01	0.12*	−0.09	0.09*
	CNRM	Whole	0.02	0.03*	−0.06	0.26*
		South	0.00	0.02	0.00	0.31*
		North	0.03	0.04*	−0.12	0.21*
Africa	ICTP_AF		0.15	0.05*	−0.23	0.25*
	ICTP_NW		−0.01	0.03	0.15	0.29*
	HC_NW		0.27	0.15*	−0.24	0.15*
East Asia	ICTP		0.20*	0.09*	0.15	0.07*
	CMA		0.05	0.15*	0.13	0.00
North America	SFU		0.00	0.05*	−0.02	0.25*

model projections (Meehl et al. 2007a). Moreover, the oceans tend to warm at a slower rate than the atmosphere (Meehl et al. 2007a), which would tend to decrease the ocean–air temperature gradient that determines evaporation. Therefore, a relatively long ''recharge time'' (and thus longer dry periods) would be needed for this moisture source to replenish the atmosphere to the local saturation levels necessary for precipitation, thereby yielding longer dry periods.

Figure 4 shows the global water budget of the ECHAM5 simulation. The ECHAM5 model shows a global surface warming trend of approximately 3.475°C $(100\ \text{yr})^{-1}$ and an atmospheric moisture increase of approximately 30% $(100\ \text{yr})^{-1}$, or about 8.7% per degree of (surface) warming. This value is in rough agreement with the C–C estimate given that the tropical troposphere warms more than the surface (in agreement with the CMIP3 ensemble; Solomon et al. 2007). The intensity of the 95th percentile precipitation events increases by about 5.44% $(°C)^{-1}$ of warming in the ECHAM5 experiment (a sub-C–C response), while precipitation intensity, which also includes lighter events, increases at a somewhat slower rate of about 16% $(100\ \text{yr})^{-1}$, or 4.58% $(°C)^{-1}$ of warming. The fact that the characteristics of changing precipitation intensities are governed by complex changes in atmospheric dynamics, thermal stability, and cloud microphysics, the details of which vary substantially across regions and model parameterizations, likely determines this global sub-C–C response (Pall et al. 2007; O'Gorman and Schneider 2009).

Mean precipitation increases by about 7.5% $(100\ \text{yr})^{-1}$ in the ECHAM5 simulation, or about 2.16% $(°C)^{-1}$ of warming, which is less than half of the trend in intensity. This trend is tied to the rate of increase of surface evaporation, which is about 2.04% $(°C)^{-1}$ of warming. The imbalance between the increase in precipitation intensity and mean precipitation therefore leads to an increase of dry spell length of about 17% $(100\ \text{yr})^{-1}$, or 4.78% $(°C)^{-1}$ of warming. The results shown in Fig. 4 thus suggest that while an increase in precipitation intensity is driven by the greater atmospheric moisture holding capacity, a less pronounced increase in mean precipitation is driven by a correspondingly lower increase in surface evaporation, which eventually results in greater dry spell lengths. These interactions within the global hydrologic cycle leading to increasing HY-INT are schematically depicted in Fig. 4c and support the interpretation of an increase in HY-INT as a signature of hydroclimatic response to global warming.

4. Response of HY-INT in the late-twentieth-century observational record

Given the robustness of increasing HY-INT in response to global warming for the A1B scenario simulations, in this section we investigate whether increasing HY-INT can also be seen in precipitation observations from the late twentieth-century decades. As mentioned in section 2, we employ a range of station and gridded observation datasets of daily precipitation, with emphasis on the 1976–2000 period. Figure 5 reports the HY-INT trends, both at the station–gridpoint level and when averaged over the different continental regions analyzed. Table 6 reports the corresponding trends in INT and DSL separately along with the HY-INT trend.

Figure 5 shows that, although some spatial variability exists within each region, an overall positive HY-INT trend is found over all regions except Australia (negative trend) and South America (negligible trend). We note in particular the large and statistically significant HY-INT trends over Europe, India, and East Asia, regions that also exhibited relatively large trends in the twenty-first-century projections. Table 6 also shows that, consistent with the twenty-first-century projections, the increase in precipitation intensity dominates in determining the HY-INT trend over northern Europe and the increase of dry spell length over southern Europe. Over the other regions, the trends of INT and DSL have varying signs, although they do combine to produce predominantly positive HY-INT trends.

As mentioned, to assess the sensitivity of the trends to the choice of analysis period, we also calculated continental-scale trends in observed HY-INT, INT, and

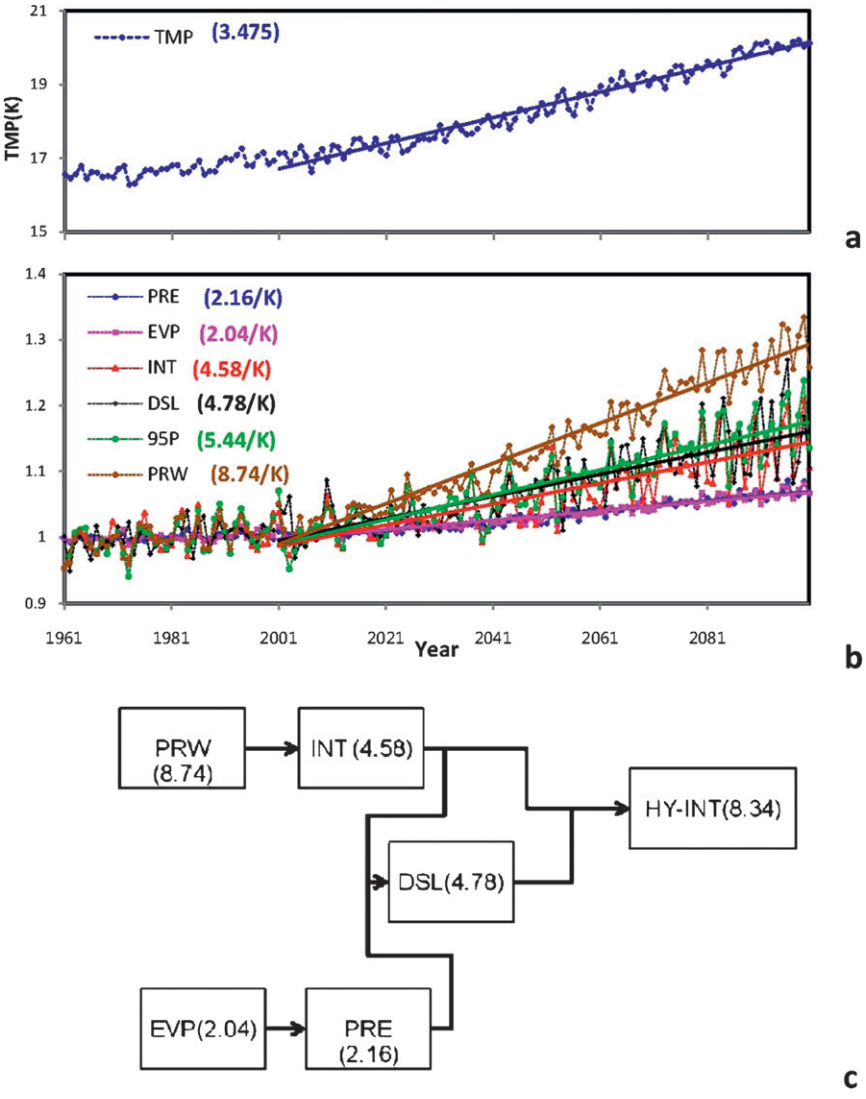

FIG. 4. Changes in the hydrologic cycle related to the HY-INT response to global warming: (a) temporal evolution (1961–2100) and linear trends (2001–2100) of globally averaged TMP; (b) normalized PRE, EVP, INT, DSL, mean precipitation intensity above the 95th percentile (95P), and precipitable water (PRW) for the ECHAM5 A1B simulation. The linear trend lines and corresponding linear trend coefficients (in the legend) are shown for each variable (units are percent increase per degree of global warming). (c) An illustrative depiction of the interrelations across the different components of the hydrologic cycle. The numbers in the boxes of (c) indicate the percent increase of the corresponding quantity per degree of global warming.

DSL for the periods 1970–2000 and 1960–2000 (Table 6). It can be seen that except for the Australia and India regions, there is good consistency among trends across the analysis periods, especially between the 1970–2000 and 1976–2000 periods. It is also clear from Fig. 5 that before the 1970s substantial trends in HY-INT are generally not found, so that the increasing HY-INT signature is particularly evident only for the later decades of the century.

For the sake of completeness, we also calculated HY-INT trends from the National Centers for Environmental Prediction (NCEP) and 40-yr European Centre for Medium-Range Weather Forecasts (ECMWF) Re-Analysis (ERA-40) data (Fig. 6; Table 7). We note that after 1975 the use of satellite data in the assimilation procedure leads to a general improvement of the reanalysis products (Simmons et al. 2004). However, as stressed by one of the anonymous reviewers, both reanalysis products are still affected by substantial errors in their representation of the hydrological cycle, particularly over tropical regions (Kinter et al. 2004; Trenberth et al. 2001;

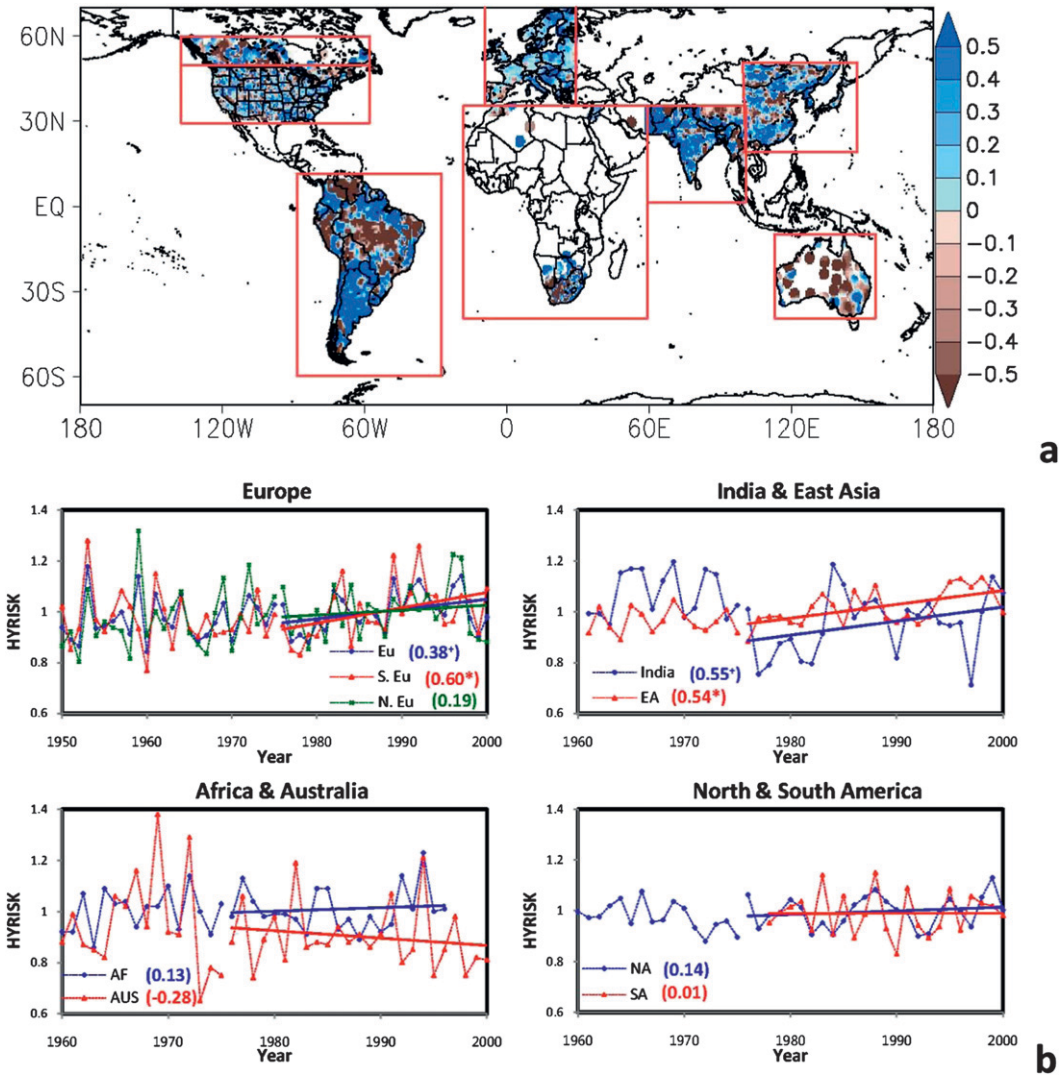

FIG. 5. HY-INT trends from observations: (a) spatial distribution of the late twentieth-century (1976–2000) linear trend of HY-INT derived from different regional observation datasets; (b) temporal evolution of HY-INT averaged over each region. Gridded datasets are used for Europe, India, East Asia, and South America, while a GCOS station dataset is used over North America (2551 stations), Africa (460 stations), and Australia (59 stations) (see Table 2). Note the strongly uneven station density in the latter two cases. Only stations with at least 300 days of data per year for the full 1976–2000 period are used in the analysis. The linear trend lines for the 1976–2000 period are shown for each region. The legend indicates the linear trend coefficient for 1976–2000 and the asterisk (cross) denotes statistical significance at the 95% (90%) confidence level. Note that all available years are shown for each dataset up to the year 2000.

Trenberth and Guillemot 1998; Newman et al. 2000). For example, a serious bias in hydrological quantities was found in ERA-40 in relation to the Pinatubo eruption of 1991, which caused significant artificial shifts in some of the assimilated satellite streams and reanalyzed precipitation fields (Uppala et al. 2005). In many regions the associated artificial hydrological shifts exceeded natural trends during the reanalysis period (Bengtsson et al. 2004; Schiemann et al. 2008). For these reasons, we stress that it is premature to use the reanalysis products for hydroclimatic monitoring and detection purposes.

On the other hand, we can compare the reanalysis data with the observed data as a validation exercise. Figure 6 shows that the spatial pattern of HY-INT trends in the NCEP reanalysis is noisy and does not show any systematic relation with the station-based trends seen in Fig. 5 (similar results were found for ERA-40). However, both reanalysis products indicate a positive global trend and mostly positive regional trends for the 1976–2000 period. Agreement with observations in producing a positive HY-INT trend is found over Europe, East Asia, and North America, while agreement of a negative trend

TABLE 6. Linear trend coefficients of normalized INT, DSL, and HY-INT in the observed datasets analyzed here (see Table 2) for the periods 1960–2000, 1970–2000, and 1976–2000 averaged over the continental regions of Fig. 5 (land only). Here, the asterisk and cross indicate that the trends are statistically significant at the 95% and 90% confidence levels, respectively.

		INT			DSL			HY-INT		
		1960–2000	1970–2000	1976–2000	1960–2000	1970–2000	1976–2000	1960–2000	1970–2000	1976–2000
Europe	Whole	0.00	0.04	0.09	0.24*	0.24	0.29	0.23*	0.26^{+}	0.38^{+}
	South	−0.14*	−0.09	0.00	0.47*	0.54*	0.64*	0.31*	0.42*	0.60*
	North	0.12*	0.15*	0.18*	0.03	−0.02	0.00	0.15	0.12	0.19
India		−0.12*	−0.08	−0.01	−0.16	0.00	0.53^{+}	−0.28	−0.01	0.55^{+}
East Asia		-0.11^{+}	−0.06	0.10	0.42*	0.52*	0.42*	0.33*	0.47*	0.54*
Africa		0.14	−0.15	−0.17	−0.04	0.15	0.27	0.09	0.01	0.13
Australia		0.03	0.04	0.13	−0.31	−0.19	−0.48	−0.27	−0.13	−0.28
North America		0.14*	0.13*	0.14^{+}	0.01	0.24	0.17	0.07	0.25*	0.14
South America				0.04			0.01			0.01

is found over Australia. NCEP and station observations both show positive trends over India and Africa, while ERA-40 shows negative trends. Further, both reanalysis products diverge from observations over South America. Comparison across global and continental HY-INT trends for the 1976–2000, 1970–2000, and 1960–2000 periods (Table 7) shows good consistency for the NCEP reanalysis, but poor for ERA-40.

These mixed results, especially in ERA-40, suggest that improved reanalysis products are needed for hydroclimatic trend detection. We also note that HY-INT shows very large fluctuations in the reanalysis products prior to 1976, a behavior that likely reflects the poorer quality of the reanalyzed precipitation fields in the presatellite era.

A general comparison of the observed trends with the corresponding trends from the climate model simulations (Figs. 2 and 3) shows that globally all datasets indicate a positive HY-INT trend over the 1976–2000 period. The increase in HY-INT in the late twentieth century could therefore serve as a valuable topic for subsequent climate change detection–attribution work. However, the global trends in the models are smaller than in the observations, and there is only a mixed agreement between models and observations at the continental scale. The mismatches between the models and observations have a number of potential causes, including physical errors in the climate models and internal climate system variability that is not captured by the small number of realizations analyzed for each model. As in the case of the reanalysis, the HY-INT metric could serve as a valuable target for climate model evaluation and improvement.

5. Discussion and conclusions

In this paper we introduce a new index, HY-INT, which combines precipitation intensity, INT, and dry spell length, DSL, as a measure of the integrated response of the hydrologic cycle to global warming. A few caveats concerning HY-INT should be highlighted. First, HY-INT is not intended to be an index of hydroclimatic extremes, such as drought or flood, and in particular it is not intended to capture specific short-term events. Rather, it is a statistical measure of the strength of the hydrologic cycle as reflected by precipitation intensity and the length of dry spells. As shown in Fig. 1, HY-INT is, however, capable of capturing the signature of exceptionally dry and/or wet conditions, such as those that occurred in the summer of 2003 over Europe.

HY-INT integrates the two hydroclimatic metrics, INT and DSL, considering them as providing an interconnected response of the earth's hydrologic cycle. An increase of HY-INT with global warming should imply that, for example, in the absence of large changes in mean precipitation both the precipitation intensity and the length of dry periods should increase in an interconnected fashion. On the other hand, in the presence of large changes in mean precipitation, the increase in one metric would overwhelm an eventual decrease in the other, so that HY-INT would still increase with warming conditions. Therefore the HY-INT signal is more ubiquitous and generally of greater magnitude compared to that of the individual metrics, thereby providing a more powerful signature of the response of the hydrologic cycle to global warming. HY-INT can also be physically interpreted as relating precipitation intensity during wet periods to the length of dry and wet spells, thereby providing valuable information on changes in the processes regulating the earth's hydrologic cycle.

Our analysis of global and regional climate model projections supports the hypothesis that the increase in HY-INT is a consistent and ubiquitous hydroclimatic signature of GHG-induced global warming, both at the global and continental scales. To place this result within the context of the global hydrologic cycle response, we analyzed the hydrologic cycle of the ECHAM5 global

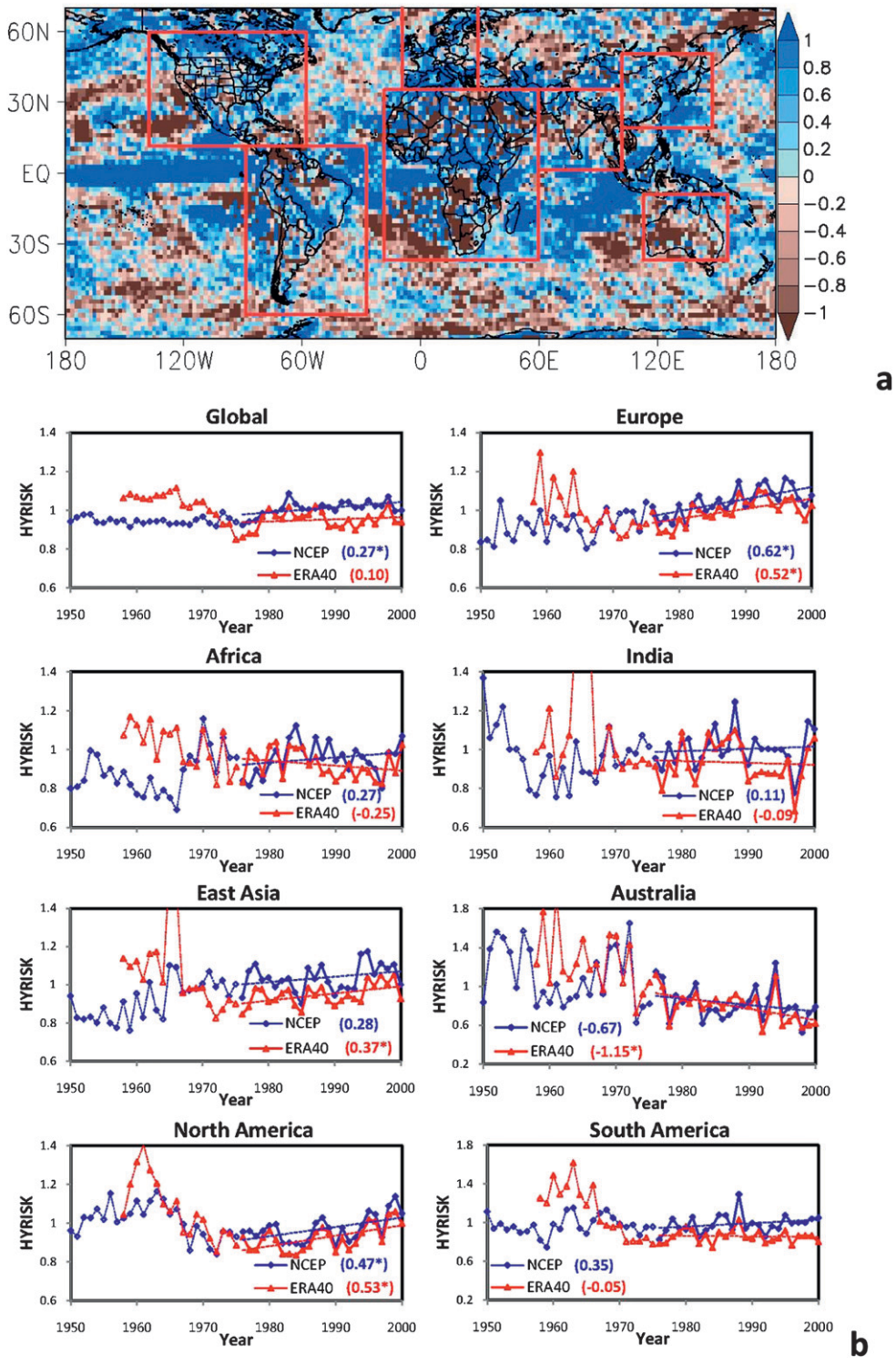

FIG. 6. HY-INT trends from reanalysis data: (a) spatial distribution of the late twentieth-century (1976–2000) linear trend of HY-INT derived from the NCEP reanalysis (Kalnay et al. 1996); (b) temporal evolution of HY-INT in the NCEP reanalysis and ERA-40 (Uppala et al. 2005) averaged over each continental region shown in (a). The legend indicates the linear trend value for 1976–2000 and the asterisk (cross) denotes statistical significance at the 95% (90%) confidence level. Note that although the trends are calculated for 1976–2000, all available years are shown up to the year 2000.

TABLE 7. Linear trend coefficients of normalized INT, DSL, and HY-INT in the NCEP reanalysis and ERA-40 for the periods 1960–2000, 1970–2000, and 1976–2000 averaged globally and over the continental regions of Fig. 6 (land only). Here, the asterisk and cross indicate that the trends are statistically significant at the 95% and 90% confidence levels, respectively.

	NCEP INT			NCEP DSL			NCEP HY-INT		
	1960–2000	1970–2000	1976–2000	1960–2000	1970–2000	1976–2000	1960–2000	1970–2000	1976–2000
Global	0.04	0.19*	0.25*	0.24*	0.17*	0.03	0.30*	0.32*	0.27*
Europe	−0.03	−0.08	−0.08	0.63*	0.69*	0.74*	0.58*	0.57*	0.62*
Africa	−0.46*	−0.08	0.06	0.78*	0.14	0.16	0.41*	−0.05	0.27
India	0.13*	−0.06	−0.17*	0.17	0.23	0.36	0.31	0.13	0.11
East Asia	−0.11^{+}	0.03	0.07	0.36*	0.18	0.17	0.31*	0.24^{+}	0.28
Australia	0.55*	0.51*	0.65*	−1.33*	−0.72*	−1.23*	−0.81*	−1.23*	−0.67
North America	0.18*	0.22*	0.19*	−0.28*	0.22*	0.28	−0.09	0.42*	0.47*
South America	0.25*	0.14*	0.14^{+}	−0.29*	0.15	0.17	−0.01	0.29^{+}	0.35
	ERA-40 INT			ERA-40 DSL			ERA-40 HY-INT		
	1960–2000	1970–2000	1976–2000	1960–2000	1970–2000	1976–2000	1960–2000	1970–2000	1976–2000
Global	0.15*	0.24*	0.31*	−0.47*	−0.19	−0.18	−0.30*	0.02	0.10
Europe	0.00	−0.06	0.02	0.12	0.61*	0.51*	0.13	0.55*	0.52*
Africa	−0.26*	−0.43*	−0.46*	−0.14	0.19	0.17	−0.42*	−0.25	−0.25
India	0.04	0.16*	0.11	−0.71*	−0.21	−0.17	−0.67*	−0.05	−0.09
East Asia	−0.19*	0.04	0.23*	−0.27^{+}	0.28*	0.12	−0.46*	0.33*	0.37*
Australia	0.07	−0.02	−0.13	−2.23*	−1.69*	−1.21*	−1.89*	−1.65*	−1.15*
North America	0.33*	0.19*	0.20*	−0.96*	0.07	0.33*	−0.54*	0.25^{+}	0.53*
South America	0.37*	0.06	−0.11^{+}	−1.74*	−0.05	−0.02	−1.16*	0.02	−0.05

climate model projection. We found that the warming-induced increase in precipitation intensity is modulated by the increase in atmospheric water holding capacity, while the mean precipitation change is associated with a less pronounced increase in evaporation. The combination of these two responses results in a greater length of dry spells and thus, in combination with greater precipitation intensity, enhanced HY-INT. We stress that the intensification of the hydrologic cycle manifesting itself with less frequent and more intense events is not a trivial fact, and might thus provide some guidance into a deeper understanding of the mechanisms determining the response of the earth's water cycle to global warming. Future research should be aimed at an even broader suite of observational and climate model data, and a deeper investigation of the physical mechanisms underlying this HY-INT response. In addition, the importance of forcings other than GHG should be examined. For example, the effect of atmospheric aerosols can be highly relevant (e.g., Trenberth and Dai 2007; Wild et al. 2008), stemming from the fact that aerosols can affect solar radiation, and thus surface evaporation and convection, as well as cloud microphysics.

Our analysis of precipitation observations shows that by and large the observed record is characterized by an increasing HY-INT signature over the last decades of the twentieth century, when global warming exhibits the largest rate of change and has been firmly attributed to anthropogenic increases in GHG concentrations (Solomon et al. 2007). This signature could therefore provide new evidence of anthropogenic influence on the climate system, and the HY-INT index can potentially provide a powerful tool in detection and attribution studies of changes in the hydrologic cycle. Further, as an integrated measure of precipitation intensity and dry spell length, HY-INT can also be considered a metric of hydroclimatic stress. In this function it could be used in impact and adaptation studies, with an increase in HY-INT implying higher hydroclimatic stress from the combined increase of flood and/or drought potential (as implied in Fig. 1). Given the potential applications and implications of these initial HY-INT analyses, we plan to extend this work to the new generation of global and regional climate model simulations of the twentieth and twenty-first centuries planned in support of the IPCC Fifth Assessment Report and to investigate in greater detail the physical processes underlying the HY-INT response.

Acknowledgments. We thank two anonymous reviewers for their useful comments, which helped to improve the quality of this manuscript. We also thank ENSEMBLES, CMIP3, and WMO for making available their data.

REFERENCES

Allan, R. P., and B. J. Soden, 2008: Atmospheric warming and the amplification of precipitation extremes. *Science,* **321,** 1481–1484.

Allen, M. R., and W. J. Ingram, 2002: Constraints on the future changes in climate and the hydrological cycle. *Nature,* **419,** 224–232.

Barredo, J. I., 2007: Major flood disasters in Europe: 1950-2005. *Nat. Hazards,* **42,** 125–148.

Bates, B. C., W. Z. Kundiewicz, S. Wu, and J. P. Palutikof, Eds., 2008: Climate change and water. IPCC Tech. Paper, Cambridge University Press, 210 pp.

Bengtsson, L., K. I. Hodges, and S. Hagemann, 2004: Sensitivity of the ERA40 reanalysis to the observing system: Determination of the global atmospheric circulation from reduced observations. *Tellus,* **56A,** 456–471.

Beniston, M., 2004: The 2003 heat wave in Europe: A shape of things to come? An analysis based on Swiss climatological data and model simulations. *Geophys. Res. Lett.,* **31,** L02202, doi:10.1029/2003GL018857.

Christensen, J. H., and O. B. Christensen, 2003: Climate modeling: Severe summertime flooding in Europe. *Nature,* **421,** 805–806.

Dai, A., K. E. Trenberth, and T. R. Karl, 1998: Global variations in drought and wet spells: 1900-1995. *Geophys. Res. Lett.,* **25,** 3367–3370.

——, ——, and T. Qian, 2004: A global dataset of Palmer Drought Severity Index for 1870–2002: Relationship with soil moisture and effects of surface warming. *J. Hydrometeor.,* **5,** 1117–1130.

Diffenbaugh, N. S., and M. Ashfaq, 2010: Intensification of hot extremes in the United States. *Geophys. Res. Lett.,* **37,** L15701, doi:10.1029/2010GL043888.

Giorgi, F., 2008: A simple equation for regional climate change and associated uncertainties. *J. Climate,* **21,** 1589–1604.

——, and E. Coppola, 2007: European Climate-Change Oscillation (ECO). *Geophys. Res. Lett.,* **34,** L21703, doi:10.1029/2007GL031223.

Haylock, M. R., N. Hofstra, A. M. G. Klein Tank, E. J. Klok, P. D. Jones, and M. New, 2008: A European daily high-resolution gridded data set of surface temperature and precipitation for 1950–2006. *J. Geophys. Res.,* **113,** D20119, doi:10.1029/2008JD010201.

Held, I. M., and B. J. Soden, 2006: Robust responses of the hydrological cycle to global warming. *J. Climate,* **19,** 5686–5699.

Hennessy, K. J., J. M. Gregory, and J. F. B. Mitchell, 1997: Changes in daily precipitation under enhanced greenhouse conditions. *Climate Dyn.,* **13,** 667–680.

Im, E. S., I. W. Jung, and D. H. Bae, 2011: The temporal and spatial structures of recent and future trends in extreme indices over Korea from a regional climate projection. *Int. J. Climatol.,* **31,** 72–86, doi:10.1002/joc.2063.

Kalnay, E., and Coauthors, 1996: The NCEP/NCAR 40-Year Reanalysis Project. *Bull. Amer. Meteor. Soc.,* **77,** 437–471.

Kinter, J. L., M. L. Fennessy, V. Krishnamurty, and L. Marx, 2004: An evaluation of the apparent interdecadal shift in the tropical divergent circulation in the NCEP–NCAR reanalysis. *J. Climate,* **17,** 349–361.

Lenderink, G., and E. Van Meijgaard, 2008: Increase in hourly precipitation extremes beyond expectations from temperature changes. *Nat. Geosci.,* **1,** 511–514.

Luterbacher, J., D. Dietrich, E. Xoplaki, M. Grosjean, and H. Wanner, 2004: European seasonal and annual temperature variability, trends, and extremes since 1500. *Science,* **303,** 1499–1503.

Meehl, G. A., J. M. Arblaster, and C. Tebaldi, 2005: Understanding future patterns of increased precipitation intensity in climate model simulations. *Geophys. Res. Lett.,* **32,** L18719, doi:10.1029/2005GL023680.

——, and Coauthors, 2007a: Global climate projections. *Climate Change 2007: The Physical Science Basis,* S. Solomon et al., Eds., Cambridge University Press, 747–846.

——, C. Covey, K. E. Taylor, T. Delworth, R. J. Stouffer, M. Latif, B. McAvaney, and J. F. B. Mitchell, 2007b: The WCRP CMIP3 multimodel dataset: A new era in climate change research. *Bull. Amer. Meteor. Soc.,* **88,** 1383–1394.

Nakicenovic, N., and R. Swart, Eds., 2000: Special report on emission scenarios. IPCC Special Rep., Cambridge University Press, 570 pp.

Newman, M., P. D. Sardeshmukh, and J. W. Bergman, 2000: An assessment of the NCEP, NASA, and ECMWF reanalyses over the tropical west Pacific warm pool. *Bull. Amer. Meteor. Soc.,* **81,** 41–48.

O'Gorman, P. A., and T. Schneider, 2009: The physical basis for increases in precipitation extremes in simulations of twenty-first-century climate change. *Proc. Natl. Acad. Sci. USA,* **106,** 14 773–14 777.

Pal, J. S., and Coauthors, 2007: The ICTP RegCM3 and RegCNET: Regional climate modeling for the developing world. *Bull. Amer. Meteor. Soc.,* **88,** 1395–1409.

Pall, P., M. R. Allen, and D. A. Stone, 2007: Testing the Clausius–Clapeyron constraint on changes in extreme precipitation under CO_2 warming. *Climate Dyn.,* **28,** 351–363.

Salinger, M. J., and G. M. Griffiths, 2001: Trends in New Zealand daily temperature and rainfall extremes. *Int. J. Climatol.,* **21,** 1437–1452.

Schär, C., P. L. Vidale, D. Lüthi, C. Frei, C. Häberli, M. A. Liniger, and C. Appenzeller, 2004: The role of increasing temperature variability in European summer heatwaves. *Nature,* **427,** 332–336.

Schiemann, R., D. Luthi, P. L. Vidale, and C. Schär, 2008: The precipitation climate of Central Asia – Intercomparison of observational and numerical data sources in a remote region. *Int. J. Climatol.,* **28,** 295–314.

Silva, V. B. S., V. E. Kousky, W. Shi, and R. W. Higgins, 2007: An improved historical daily precipitation analysis for Brazil. *J. Hydrometeor.,* **8,** 847–861.

Simmons, A. J., and Coauthors, 2004: Comparison of trends and low-frequency variability in CRU, ERA-40, and NCEP/NCAR analyses of surface air temperature. *J. Geophys. Res.,* **109,** D24115, doi:10.1029/2004JD005306.

Solomon, S., D. Qin, M. Manning, M. Marquis, K. Averyt, M. M. B. Tignor, H. L. Miller Jr., and Z. Chen, Eds., 2007: *Climate Change 2007: The Physical Science Basis*. Cambridge University Press, 996 pp.

Sugiyama, M., H. Shiogama, and S. Emori, 2010: Precipitation extreme changes exceeding moisture content increases in MIROC and IPCC climate models. *Proc. Natl. Acad. Sci. USA,* **107,** 571–575.

Tebaldi, C., K. Hayhoe, J. M. Arblaster, and G. A. Meehl, 2006: Going to the extremes: An intercomparison of model-simulated historical and future changes in extreme events. *Climatic Change,* **79,** 185–211.

Trenberth, K. E., 1999: Conceptual framework for changes of extremes of the hydrological cycle with climate change. *Climatic Change,* **42,** 327–339.

——, and C. J. Guillemot, 1998: Evaluation of the atmospheric moisture and hydrological cycle in the NCEP-NCAR reanalyses. *Climate Dyn.,* **14,** 213–231.

——, and A. Dai, 2007: Effects of Mount Pinatubo volcanic eruption on the hydrological cycle as an analog of geoengineering. *Geophys. Res. Lett.,* **34,** L15702, doi:10.1029/2007GL030524.

——, D. P. Stepaniak, J. W. Hurrell, and M. Fiorino, 2001: Quality of renalyses in the tropics. *J. Climate,* **14,** 1499–1510.

——, A. Dai, R. Rasmussen, and D. Parsons, 2003: The changing character of precipitation. *Bull. Amer. Meteor. Soc.,* **84,** 1205–1217.

Uppala, S. M., and Coauthors, 2005: The ERA-40 Re-Analysis. *Quart. J. Roy. Meteor. Soc.,* **131,** 2961–3012.

Wild, M., J. Grieser, and C. Schär, 2008: Combined surface solar brightening and increasing greenhouse effect support recent intensification of the global land-based hydrological cycle. *Geophys. Res. Lett.,* **35,** L17706, doi:10.1029/2008GL034842.

Yatagai, A., O. Arakawa, K. Kamiguchi, H. Kawamoto, M. I. Nodzu, and A. Hamada, 2009: A 44-year daily gridded precipitation dataset for Asia based on a dense network of rain gauges. *SOLA,* **5,** 137–140.